couple to the far field. On the other hand, the TE_{41} and TM_{11} modes have propagation lengths shorter than 1 μm and cannot be transmitted to the far field. This is likely due to the noble metals electrodes being lossy in the blue region of the visible spectrum. In Table 1 we present the maximum propagation length of each mode at the wavelength where it occurred. As expected, the propagation length decays strongly when the excitation wavelength approaches to the cutoff wavelength because the specific modes become evanescent. In Fig. 3(b), such values are nonzero because of the finite number of frequency steps used in our calculations.

Table 1. Maximum propagation length for each studied mode

	Mode					
	TEM	TE_{11}	TE_{21}	TE_{31}	TE_{41}	TM_{11}
Maximum propagation length (μm)	∞	9.27 μm @1.28 μm	5.61 μm @0.84 μm	3.43 μm @0.69 μm	0.96 μm @0.58 μm	0.81 μm @0.6 μm

Finally, in order to complete the optical characterization of the nanocoax array, we measured experimentally the transmittance of the sample as a function of the excitation wavelength using a fiber optic spectrometer (Ocean Optics 2000) attached to an optical microscope (Leica 6000M) at the image plane. The illumination sources were the same as the NSOM experiment, plus a broad spectrum white light emitting diode (LED). The experimental transmittance was defined as the ratio between the output intensity (after background subtraction) and the input intensity in percentage units, i.e., $T = 100\ (I_{out} - I_{bkg})/I_{in}$, where I_{out} is the transmitted intensity, I_{bkg} the background intensity and I_{in} the intensity in the absence of sample, *i.e.* the emission spectrum of the source. Figure 4 shows the experimentally-measured transmittance with white LED source (black line) and monochromatic sources (green figures), along with the calculated transmittance (red line). The later was obtained by using the same model as for the calculation of propagating fields inside the nanocoax.

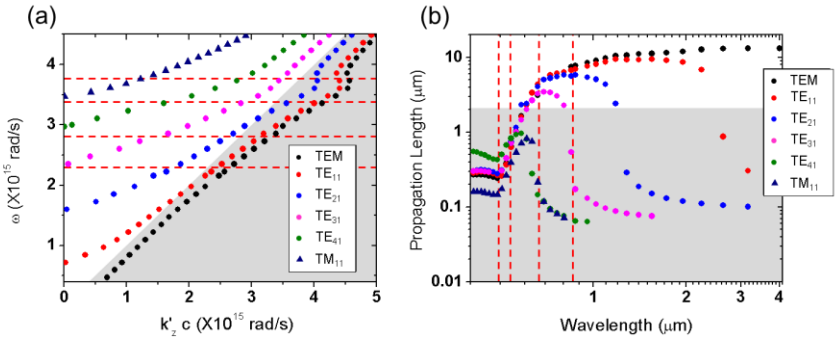

Fig. 3. (a) Calculated dispersion relations of the modes propagating in the nanocoax structure. The dashed lines represent the frequencies employed (excitation wavelengths) and the shaded zone represents the zone where plasmonic modes appear (i.e. separated from photonic modes by the light line ω = kc). (b) Calculated propagation lengths for the studied modes. The dashed lines represent the wavelengths used and the shaded zone indicates the length *L* of the nanocoax structure. Note the logarithmic scales.

It is clear that the transmittance is dominated by several peaks, at 761 nm and 874 nm in the calculated result and 591 nm and 647 nm in both measured and calculated results. These peaks can be explained as follows: in the coaxial structure, the propagating modes appear in three dimensions, *i.e.* radial, azimuthal and longitudinal. In this way, if the coaxial structure is long enough to support Fabry-Perot resonant cavity modes, the longitudinal order mode, according to phase-matching conditions in the coaxial structure, is $2k_z'L = 2p\pi - \phi_r$, with k_z'

#210870 - $15.00 USD Received 25 Apr 2014; revised 19 May 2014; accepted 22 May 2014; published 2 Jun 2014

for each specific mode inside the coaxial cavity. Here, L is the length of the coaxial structure, p the order of the resonant mode and ϕ_r a phase shift acquired in reflections of the mode at the cavity output [31]. If ϕ_r is small enough, the resonant condition becomes $k_z' L = p\pi$. Using the length of the nanocoax structure (L), each resonant order mode was calculated. Thus, as indicated in Fig. 4, the peak at 647 nm is due to a superposition of resonant longitudinal modes with orders p = 7 and 6 of the TE_{11} and TE_{21} modes, respectively, while at 591 nm the superposition is by orders 6 and 8 of the TE_{11} and TE_{31} modes, respectively. In both cases, such superposition of modes is the reason for the strong far field transmission reported in the experimental data. The coefficients of the modes superposition were not calculated in the present work. The peaks that appear in the calculated transmittance at 761 nm and 874 nm are related to the same process and due to order p = 3 of TE_{31} and TE_{21} modes, respectively. It is important to note that the weak transmittance at wavelengths shorter than 550 nm is due to the short propagation length of all the modes, since the plasma resonance wavelength occurs around such a wavelength, resulting in highly attenuated modes, Fig. 3(b).

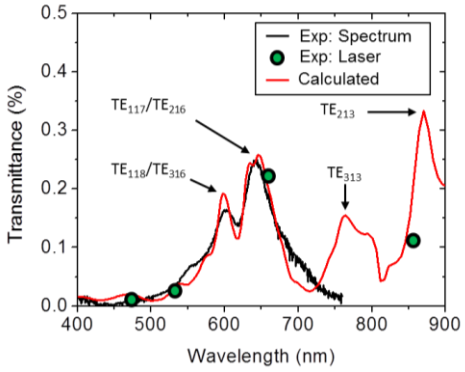

Fig. 4. Experimental (black line and green circles) and calculated (red line) transmission. Circles were obtained using single wavelength sources. The resonant modes discussed in the text are indicated.

4. Conclusions

In summary, experimental observations of plasmonic and photonic modes propagating in nanocoax structures are presented for the first time, using near-field microscopy. Comparison between NSOM experiments and calculations demonstrate that the experimental data are related to the propagating electromagnetic field in the nanocoax structure. By calculating $\boldsymbol{k}_z$ of each mode, we determined the propagation lengths and conclude that the TE_{11}, TE_{21} and TE_{31} modes can propagate along the full nanocoax length and couple to the far field, in the spectral range analyzed experimentally. These results are relevant to understanding the physics of propagated fields in nanocoax structures and their potential applications in the subwavelength nanoscale manipulation of light including, for example, polarization-preserving optical waveguides for optical communication.

Acknowledgments

This work was supported by the W. M. Keck Foundation. J.M.M. acknowledges support from CONACyT, fellowship number 203768.

#210870 - $15.00 USD Received 25 Apr 2014; revised 19 May 2014; accepted 22 May 2014; published 2 Jun 2014